Excited State Dynamics of Semiconducting Nanomaterials: Quantum Dots (CdSe) and Nanofibers (P3HT)

Ajeet Kumar
(MS14171)

A dissertation submitted for the partial fulfilment of BS-MS dual degree in Chemical Sciences

INDIAN INSTITUTE OF SCIENCE EDUCATION AND RESEARCH MOHALI

April 2019

CERTIFICATE OF EXAMINATION

This is to certify that the dissertation titled "**Excited State Dynamics of Semiconducting Nanomaterials: Quantum Dots (CdSe) and Nanofibers (P3HT)"** submitted by **Mr. Ajeet Kumar** (Reg. No. MS14171) for the partial fulfilment of BS-MS dual degree programme of the Institute, has been examined by the thesis committee duly appointed by the Institute. The committee finds the work done by the candidate satisfactory and recommends that the report be accepted.

Dr. Jino George | Dr. Sanchita Sengupta | Dr. Arijit Kumar De (Supervisor)

Date: April 26, 2019

DECLARATION

The work presented in this dissertation has been carried out by me under the guidance of Dr. Arijit Kumar De at the Indian Institute of Science Education and Research Mohali.

This work has not been submitted in part or in full for a degree, a diploma, or a fellowship to any other university or institute. Whenever contributions of others are involved, every effort is made to indicate this clearly, with due acknowledgement of collaborative research and discussions. This thesis is a bonafide record of original work done by me and all sources listed within have been detailed in the bibliography.

Ajeet Kumar

(Candidate)

Date: April 26, 2019

In my capacity as the supervisor of the candidate's project work, I certify that the above statements by the candidate is true to the best of my knowledge.

Dr. Arijit Kumar De

(Supervisor)

ACKNOWLEDGEMENTS

First of all, I would like to thank Dr. Arijit Kumar De for providing me with interesting problems to work on and for the insightful discussions to solve them.

I would like to thank Dr. Jino George, Dr. Sanchita Sengupta for their valuable scientific comments which provided great help in the project.

I would like to thank Pankaj Seliya for helping me in doing the experiments. I would also like to thank my lab members Dr. Arindam Das, Dr. Subhash Chander, Dr. Somrita Mondal (alumni) Ms.Yogita Silori, Ms. Anita Devi, Ms. Shaina Dhamija, Ms. Monika Mr. Sumit Yadav, Ms. Garima Bhutani, Ms. Sakshi Chawla, Ms. Shruthi S. Nair and Ms. Umang Gupta for their constant support, inspiration and fruitful discussions.

I would like to thank IISER Mohali for all the instrumentation facilities and the library for providing access to a plethora of journals.

And finally, to my friends (Pankaj bro.., Jorawar , Navnoor, Himanshi, Raman, Rishab, Riyaz Anupreet, Kaveri, Naman Kumar) and family for their constant motivation and support.

CONTENTS

LIST OF FIGURES

LIST OF TABLES

ABBREVIATIONS

QDs	Quantum dots
DSSC	Dye Sensitized solar cell
VB	Valence-band
NF	Nano Fibres
P3HT-NF	Poly(3-hexylthiophene-2,5-diyl) Nanofibers
TCSPC	Time-Correlated-Single Photon Counting
IRF	Instrument Response Function
TOP	Trioctylphosphine
TAS	Transient Absorption Spectroscopy
SE	Stimulated Emission
GSB	Ground State Bleach
ESA	Excited State Absorption
NOPA	Noncollinear Optical Parametric Amplifier
BBO	Beta Barium Borate (BaB_2O_4)
FT	Fourier Transformation

ABSTRACT

Nanomaterials provide lot of opportunity in improvement & new generation of photovoltaics. Their wide-bandgap are attracting an increased attention for their potential application in emerging energy. In recent year Quantum dots (QDs have emerged as a promising candidate for light harvesting and optoelectronics. QDs have opened up new ways of utilizing hot electrons and generate multiple exciton upon absorption of a single photon. On the other hand, semiconducting polymer have numerous applications in optoelectronics as well as in energy conversion. In our case we are interested in conjugaed polymer in which exciton delocalization take place up to several monomeric units upon photo excitation when they are in their aggregated forms. Here we are interested in understanding the exciton dynamics within QDs and j-aggregates of P3HT polymer nanofibers using femtosecond resolved pump-probe spectroscopy. Using this technique, we have advantages to characterize the excited state species which are formed for a very short time scale(100fs-ps) under photoexcitation. In this technique we ultrafast short pulses (<100fs) which are capable to probe these the dynamics of such species.

QUICK OVERVIEW OF THESIS

The work done in the thesis has been explained in briefly here. The detailed explanation is given in different part of the thesis.

The first chapter of thesis talk about the main technique named by 'Transient Absorption Spectroscopy' which was used to study the chemical system. This is a very strong and widely used technique to understand the excited state dynamics of molecules.

In the second chapter the process to synthesize different sized CdSe Quantum Dots is given and their surface functionalization was done in order to improve their photovoltaics compatibility and to reduce defects on their surface (which limits their photovoltaics performance). Various techniques were used in order to characterize their optical properties for example UV-Vis, Fluorescence and TCSPC. To study excited state dynamics of these systems Transient Absorption Spectroscopy was also performed.

In the third chapter the optical studies were performed for J-aggregates of P3HT polymers (P3HT-NF) which is very good candidate for photovoltaics as they show charge mobility in two directions (along the chain and between the chains) because of their specific packing behavior. In order to study the excited state dynamics Transient Absorption Spectroscopy was also performed where we were able to detect excited state species such as polaron, delocalized polarons and polaron pairs.

Chapter-1

Transient Absorption Spectroscopy

1.1 Introduction

In our work pump-probe/transient absorption spectroscopy is the main tool we have used to study the excited state dynamics of our chemical systems. In order to study photophysical and photochemical processes transient absorption spectroscopy has become a power full and widely used technique. In this technique the process which are to be investigated are triggered by exciting the molecule with ultra-short pulses. Then then dynamics of electronically excited states is probed by another light pulse that monitor the photo-induced transmission changes. Here we will learn the working and types of signals we get using the techniques in details:

It involves exciting the sample with a short laser pulse (called pump) and monitoring the changes by another time delayed pulse (called probe). The delay between the pump and the probe is varied using a mechanical delay line.

Every alternate pump pulse is blocked using a chopper running at half the frequency of the laser. The absorbance of the probe is then taken both in presence and in the absence of pump. The difference of these two absorbance gives the required transient absorption signal.

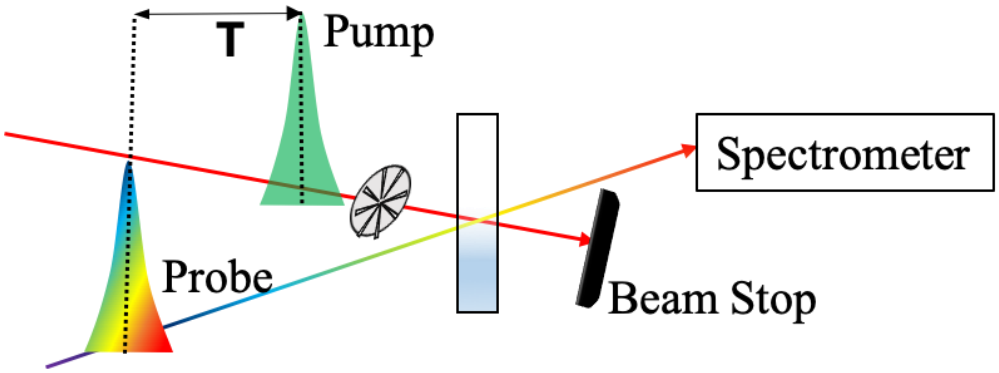

***Figure 1.1**: Schematic of a pump – probe experiment*

The differential absorption signal is given as:

$$\Delta\mathbf{A} = \mathbf{A}_{\mathbf{probe\ (pump\ on)}} - \mathbf{A}_{\mathbf{probe\ (pump\ off)}} = -\mathbf{log}\left(\mathbf{I}_{\mathbf{probe\ (pump\ on)}}\right) + \mathbf{log}\left(\mathbf{I}_{\mathbf{probe\ (pump\ off)}}\right) \quad \mathbf{(1.1)}$$

$$\Delta A = \mathbf{log}\left(\frac{\mathbf{I}_{\mathbf{probe\ (pump\ off)}}}{\mathbf{I}_{\mathbf{probe\ (pump\ on)}}}\right) \quad \mathbf{(1.3)}$$

ΔA = measured differential absorption signal

1.2 Transient absorption signals

The transient absorption signal of a molecule can contain three types of signals which are: (1) Ground State Bleach (GSB) (2) Stimulated Emission (SE) (3) Excited State Absorption (ESA).

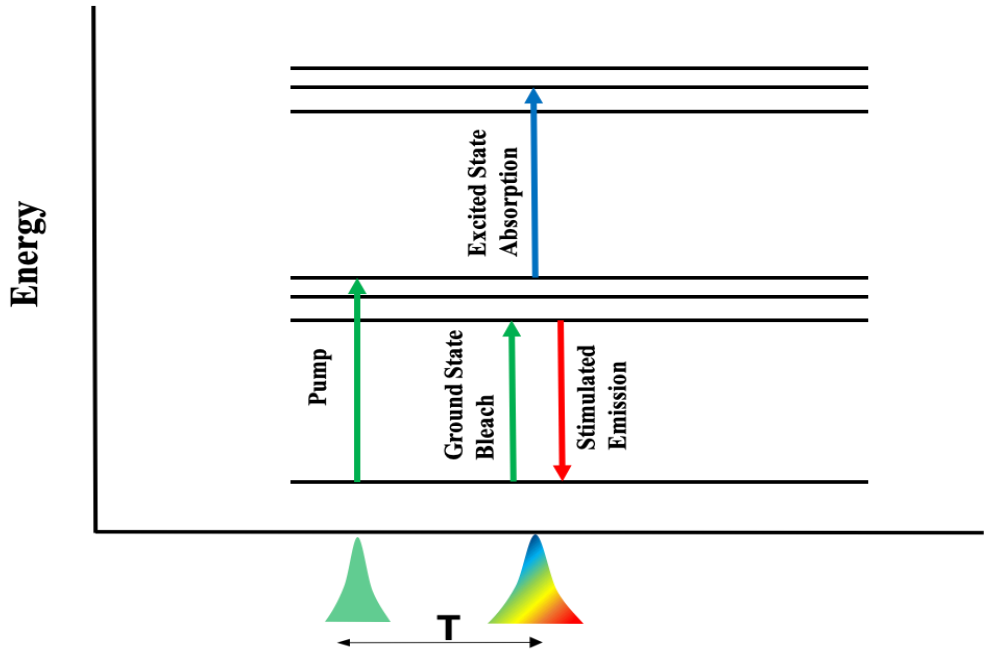

***Figure1.2**: Energy level diagram for a molecule*

1. **Ground State Bleach (GSB):** On exciting the sample with the pump, the ground state population is depleted. Therefore, the absorption of the probe at wavelength of ground state absorption is decreased and thus a negative differential absorption (ΔA) is seen. This signal is called as ground state bleach (GSB).
2. **Stimulated Emission (SE):** The probe can stimulate the population in excited state (created by pump) back to ground state. When the pump is blocked, the number of photons reaching the detector is the total photons contained in the probe. When the pump is on, the number of photons reaching the detector is the number of photons in the probe plus the photons emitted by the sample. Thus, $I_{pump\ on} > I_{pump\ off}$. Therefore a negative differential absorption (ΔA) signal is observed. This signal is called as stimulated emission (SE).
3. **Excited State Absorption (ESA):** The molecule in its excited state can absorb a photon from the probe and go to a higher lying excited state. In this case

$A_{pump\ on} > A_{pump\ off}$ and a positive differential absorption (ΔA) signal is seen. This signal is called as excited state absorption (ESA)

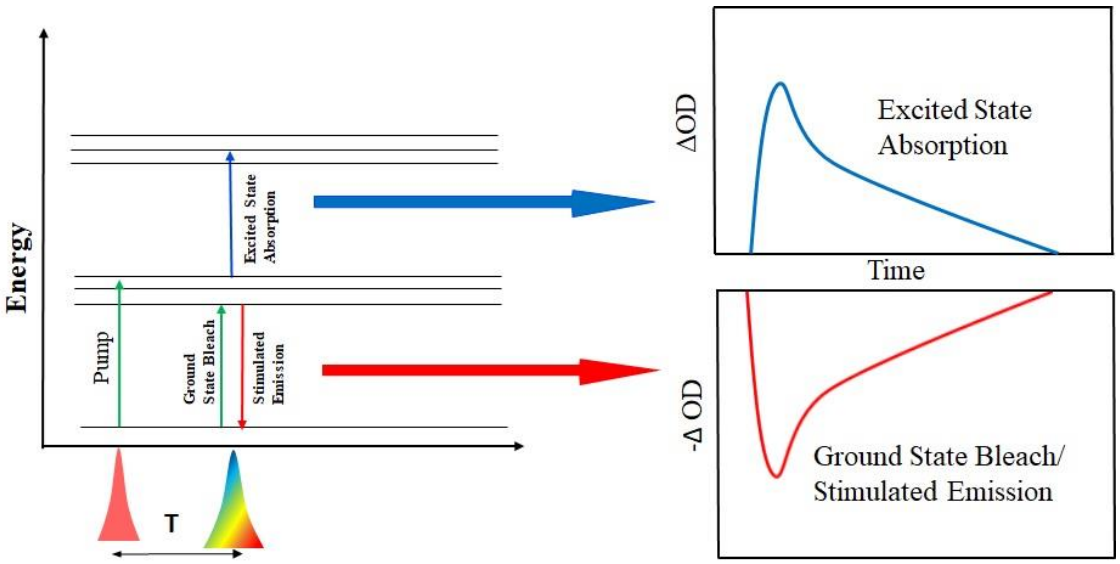

***Figure 1.3**: Types of signals in a pump – probe experiment*

1.3 Specifications of the Instrument

For our experiment Ti – Sapphire amplified laser beam was used to generate wavelength which was centred at 800 nm. The repetition rate and the pulse width of the laser was 1 kHz and 50fs respectively. In order to split the 800nm laser beam into pump and probe pulses a beam sampler was used in the path. Then probe pulse was routed to the custom-made femtosecond transient absorption spectrometer (TAS, Newport Inc, USA) which was further re-designed according to the specific requirement and pump pulse was routed toward the NOPA (Light Conversion) in order to get required wavelength for pump excitation. Probe was vertically polarized and pump was set at magic angle (54.7˚) using half wave plate in both the arms. Pump and probe power were 14.8mW and 14.3mW respectively before TAS. To generate the broad continuum of light in visible and near IR range CaF_2 crystal was used which was placed on a motorized translation stage. Intensity of probe pulse was controlled by variable neutral density filter at the sample position. 520 nm excitation wavelength was generated using NOPA. To block every alternate pump pluse a mechanical chopper (New Focus 3502, with a 7/5 slot wheel, Newport Corp) was placed

in pump arm which was operating at the 500 Hz repetition rate. Probe was spectrally overlapped with the pump beam, collimated and sent into the spectrograph (Oriel MS260i, Newport Corp). The transmitted probe pulse was detected with a spectrometer using 1200 grooves/mm grating (Richardson grating 74064, Newport Corp) with the help of a linear array detector (CMOS S10453-1024Q, Hamamatsu Photonics). The time delay between the pump and probe pulses could be varied using a mechanical delay line (ILS300LM, Newport Corp) which was controlled by the software.

Chapter-2

Excited state dynamics of CdSe Quantum Dots

2.1 Introduction

Energy is the locomotive for the economic development of modern society. Although there are enormous renewable and non- renewable energy sources but these are limited. Many of the available sources cause greenhouse effect. In order to meet the energy demand, there is a need for alternative energy sources which are environmentally friendly. There are a number of lights harvesting systems where energy transfer happens quite efficiently but when it comes to artificial light harvesting systems, there is still room to explore possibilities to get highly efficient systems.

2.1.1 Quantum Dots

There are a number of semiconductors with band gap between 0.35 and 3.5thatabsorb light over a wide range of the solar spectrum and can be used for solar cell applications. The first solar cell used silicon as the semiconductor. Preparation and installation of a silicon-based solar cell is expensive. There are many other semiconducting materials which have been used for solar cell applications like InAs, GaAs, InP, GnP. Although these are inexpensive but are less efficient than silicon based solar cells. DSSC (Dye Sensitized solar cell) show efficiency around ~10%, but undergo photobleaching in quite short time duration.[1-2]

In the past three decades, nanomaterials have emerged as the new building blocks to construct light energy harvesting assemblies. Colloidal quantum dots (QDs) have emerged as a material for a low-cost solar cell in the past decade. QD based solar cells caught a lot of attention during the past few years because of the possibility of increasing the energy conversion efficiency, as QDs have many desired properties like photostability, small bandgap, light absorption over a broad spectral range, discrete energy levels, size as well as energy-level tunability (as described by the quantum confinement property). Since QD based devices can generate multiple excitons with one photon (a 'hot' electron generated in a high conduction band by absorbing a high-energy photon relaxing to a low Conduction band, with the energy loss exciting additional electrons from valence-band (VB) to CB.[4-6] The energy conversion efficiency for QDs can go beyond the traditional Shockley and Queisser limit 32% for Si-based solar cells as the absorption of a high-energy photon creates more than one electron-hole pairs, opposite to Auger relaxation.

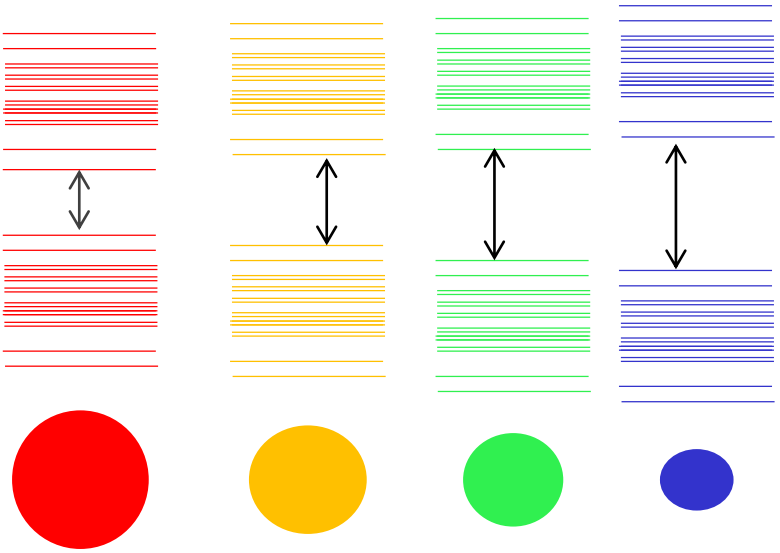

Figure.2.1*: Schematic of Size-dependent band gap of Quantum Dots.*

The size of QDs is temperature dependent. Using the hot injection method, the size of quantum dots increases with increase in temperature. There is an inverse relation between the size and band gap in QDs due to the quantum confinement property of quantum dots. QDs show size-tunable property only if they have a size within Bohr radius. The size of quantum dots, in general, is between 1- 10nm.

2.1.2 Applications of Quantum Dots

QDs have great potential for different applications due to their electronic and optical properties. QDs have been used in photovoltaic devices due to their low cost and optical properties. Electron can get transferred to a higher bandgap semiconductor (as TiO_2 and ZnO). QD based solar cells may have the advantage of carrier multiplication to increase efficiency.

QDs can also be used in Light emitting diodes (LEDs). Quantum Dots based LED TV show bright and better colour quality. They have high efficiency and low power consumption. LED bulb generates quasi-monochromatic light but more than one type of quantum dots can be used to get the white light LED.[2-3]

2.1.3 Surface passivation of CdSe QDs

QDs synthesized using solution processed hot injection method are hydrophobic so cannot be used for biological applications as these are insoluble in water. Since the ligands (Trioctylphospheneoxide, Trioctylphosphosne) used to stabilize the QDs are organic. It is possible to make QDs can be made water soluble by the surface passivation process.

Surface passivation of QDs with a higher band gap semiconductor like ZnO increase its quantum yield and fills the traps to increase the lifetime of the quantum dots. And also due to the process of surface passivation, water soluble QDs can be used for biological applications. QDs can play a more active role as an in vitro or in vivo biosensor. QDs have the potential to allow the development of FRET-based nanoscale biosensors. Using a pair of quantum dots and dye-labelled protein having spectral overlap between emission spectra of QDs and absorption spectra of dye, FRET will occur between QDs and dye (QDs being the donor and dye being the acceptor).

In this project, CdSe Quantum Dots were synthesized and cysteine was used for the passivation of CdSe QDs. Using different concentrations of cysteine, the change in lifetime of quantum dots was studied. Interestingly, after passivation with cysteine, QDs became water soluble and can be used for biological applications. On mixing cysteine with quantum dots, it replaces the bulky hydrophobic ligands from the surface of quantum dots since the thiol group of cysteine has a high affinity towards CdSe quantum dots.

2.2 Experimental Techniques

2.2.1 Steady-state absorption

The absorption spectra of different sized QDs were recorded using UV-VIS-NIR spectrophotometer (Cary 5000, Agilent). A quartz cuvette of 1 cm optical path was used for measurement and baseline was done using toluene. Optical density was managed as per the requirement by dilution. The dilution for QDs after surface modification was done in the same proportion as for the QDs without surface modification.

2.2.1.1 Determination of particle size from UV-Vis spectroscopy

To calculate the size of synthesized QDs, the equation (1) was used as given by Peng *et. al.*[7].

$$D = (1.6122\times10^{-9})\lambda^4 - (2.6575\times10^{-6})\lambda^3 + (1.6242\times10^{-3})\lambda^2 + (0.4277)\lambda + 41.57 \quad (2.1)$$

where, **D** (nm) = size of CdSe QDs and

λ = Absorption maxima of the corresponding CdSe QD nanoparticles (at first absorption peak from red side of the spectrum).

1.2.2 Fluorescence Spectroscopy

Steady-state fluorescence measurements were performed using fluorimeter (FLUOROMAX-4C, Horiba Scientific). A quartz fluorimeter cuvette of 1 cm path was used for measurements. Fluorescence spectra of CdSe QDs were recorded at excitation wavelength of 485 nm.

2.2.3 Fluorescence lifetime measurements

To determine the fluorescence lifetime from time resolved fluorescence intensity decays using a time-correlated-single photon counting (TCSPC) spectrophotometer (Fluorocube, Horiba Jobin Yvon, NJ, Edinburgh instruments) was used. A 485 nm pulsed LED excitation (pulse width < 200ps) was used to excite the sample and the data was recorded at emission maxima of the QDs. The instrument response function (IRF) was ~280ps, determined by FWHM of the

2.2.4 Transient absorption spectroscopy

Details of the technique is explained in the section 1.1.

2.2.5 Scanning Electron Microscope (SEM) Measurement:

To characterize the morphologies of the samples of P3HT-NF (details in chapter 2) by field emission scanning electron microscopy (JEOL JSM-7600F). SEM measurements were not done for CdSe QDs because of limited resolution of the instrument.

2.2.6 TEM Measurement:

TEM measurements were carried out using transmission electron microscope (JEOL-JEM-2100) with an acceleration voltage of 200 kV.

2.3 Synthesis of CdSe Quantum Dots

2.3.1 Materials Required

Selenium powder, Trioctylphosphine (TOP), 1-Octadecene, Oleic acid, Cadmium Oxide, L-Cysteine hydrochloride were purchased from Sigma Aldrich. Methanol, Sodium Hydroxide, Ethanol, Potassium hydroxide were purchased from Merck, India. Toluene, chloroform, methanol was used as solvents. All of the solvents were purchased from Sigma Aldrich, India and used without any further purification.

2.3.2 Preparation of CdSe quantum dots:

CdSe QDs were synthesized using CdO and Se. Se precursor was prepared by reducing 30 mg of Se powder. 5 mL of 1-octadecene and 0.4 mL trioctylphosphine (TOP) were added to the Se powder in a round bottom flask (RB). The solution was stirred under nitrogen atmosphere and temperature was maintained at 100˚C throughout. This mixture was stirred until selenide solution turned out to be colourless from black after reduction.

Cd precursor was prepared using Cadmium oxide. 13 mg of CdO was placed in a 50 mL RB flask loaded with 0.6 mL of oleic acid and 10 mL of octadecene. The reaction mixture was kept in constant nitrogen atmosphere. 1 mL of the previously prepared selenium solution was injected into the reaction mixture containing CdO at different temperature

(330-350^{o} C) in order to synthesize different sized QDs. After the selenide injection the reaction mixture was further stirred for 1-2 minutes, next the reaction was quenched using ice water bath. After cooling down, the as synthesized CdSe QDs were collected in vials. These synthesized CdSe QDs were purified by repetitive washing and centrifuging with ethanol and finally stored in toluene.

2.3.3 Surface functionalization of CdSe QDs with L-Cysteine:

For surface functionalization 2 nm sized CdSe QDs were used. Chemical method was used for surface functionalization with L-Cysteine hydrochloride. 5 mL oleic acid capped QDs were mixed with 5 mL L-cysteine solution in methanol of concentration 5×10^{-2} M. The mixture was kept at 40^{o} C for 24 hours and was stirred continuously. Two different coloured layers were formed, the solution was then centrifuged. The surface functionalized QDs were purified by washing and centrifugation with ethanol for multiple times.

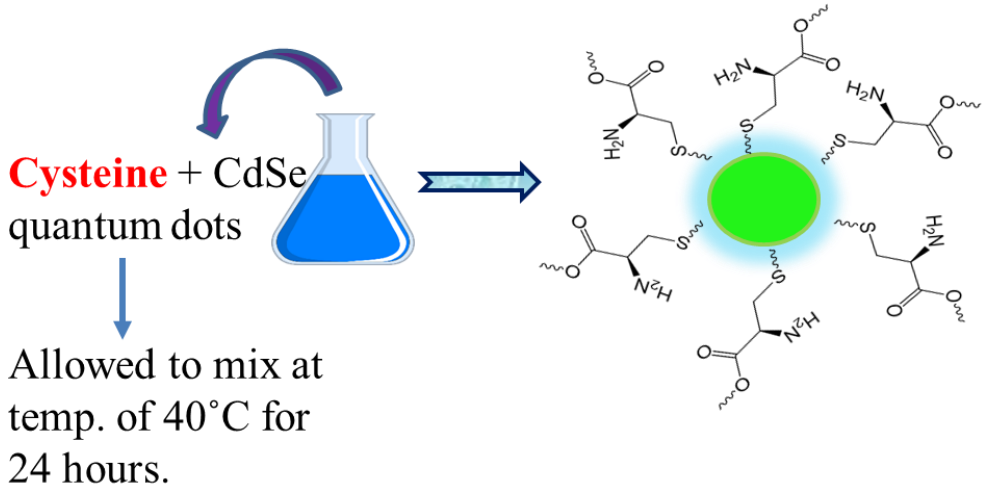

***Figure 2.2**: Schematic of synthetic procedure to link quantum dot with cysteine.*

2.4 Results and Discussion

2.4.1 Steady-state absorption of CdSe QDs:

The synthesized CdSe QDs of different sizes show absorption maxima in the range 480-620 nm range. The absorption spectra are shown in figure 2.3. Main electronic peaks are observed at 545, 565, 578, 602 nm for 2.94 nm, 3.38 nm. 3.75 nm, 4.58 nm sized QDs respectively.

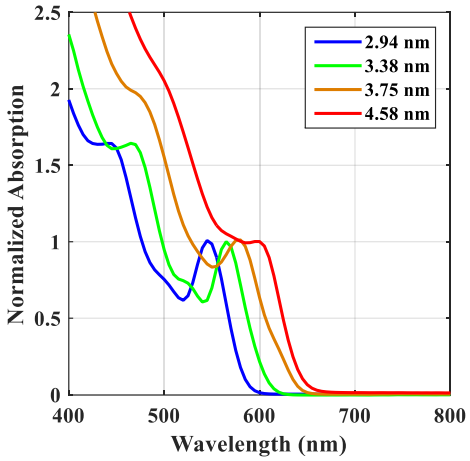

***Figure 2.3**: Steady state absorption spectra for different sized CdSe QDs.*

2.4.2 Steady-state fluorescence of CdSe QDs :

To record fluorescence spectra, QDs were excited at 485 nm. The fluorescence emission maxima are at 545 nm, 565 nm, 578 nm and 627 nm for 2.94 nm, 3.38 nm, 3.75 nm, 4.58 nm sized QDs respectively.

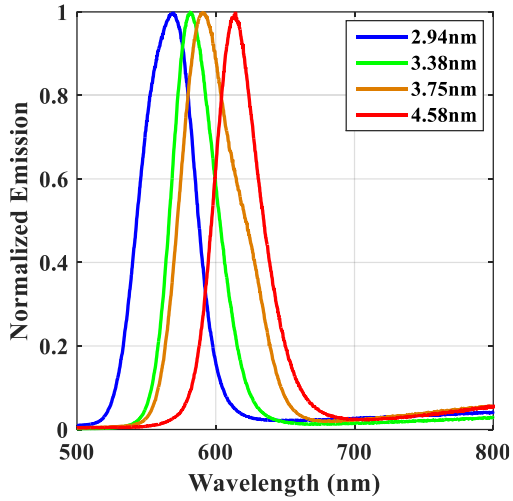

***Figure 2.4**: Steady state absorption spectra for different sized CdSe QDs*

QDs	Size(nm)	Absorption Max. (nm)	Emission Max. (nm)
1	2.94	545	560
2	3.38	565	579
3	3.75	578	594
4	4.58	600	611

***Table 2.1**: Table showing size, absorption and emission maxima for four different sized CdSe QDs.*

The fluorescence emission of QDs doesn't quench even after three months of storage. Figure 2.5 shows that the QDs are quite photostable and show very bright colour emission when illuminated even after a long time under UV light.

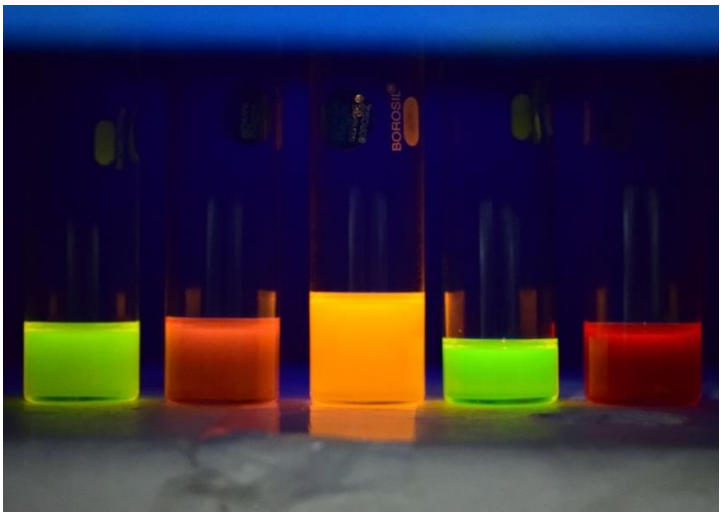

***Figure 2.5**: Luminescence from Quantum Dots of different size Under-UV light.*

2.4.3 TEM Measurements

The size of different QDs as measured using TEM is (a)1.9 nm (b) 2.8 nm (c) 3.3 nm and (d) 4 nm respectively. From HRTEM lattice fringes, it is clear that the synthasized QDs has very good crystalinity. But fringes for the highest measured size of QDs are a bit distorted (do not show perfect circle) which is indication of less crystalinity of QDs (4.58 nm). Analysis suggests that QDs have hexagonal Wurtzite structure with (101) planes.

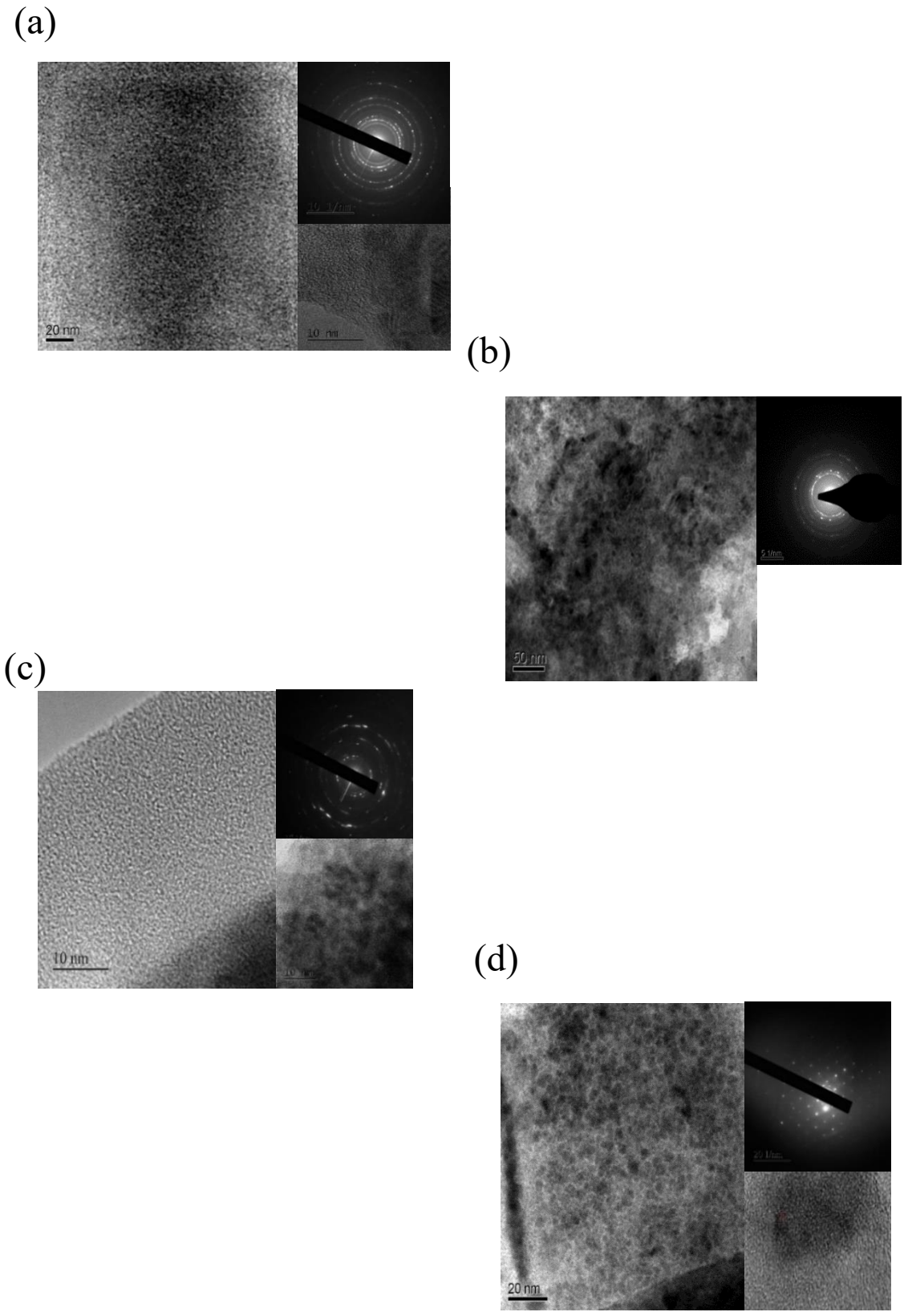

***Figure 2.6**: TEM images for different sized CdSe quantum dots (a) 2.94nm (b) 3.38nm (c) 3.75nm (d) 4.58nm.*

2.4.4 Fluorescence lifetime measurements:

The values of fluorescence lifetime for different sized QDs are shown in the table: and the decay profile is shown in figure 2.7. From the table, it is clear that the average fluorescence lifetime decreases with increase in size of QDs. This can be because of the increased trap state emission (which has longer lifetime) in smaller sized QDs or lack of surface passivation which causes surface defects in QDs.

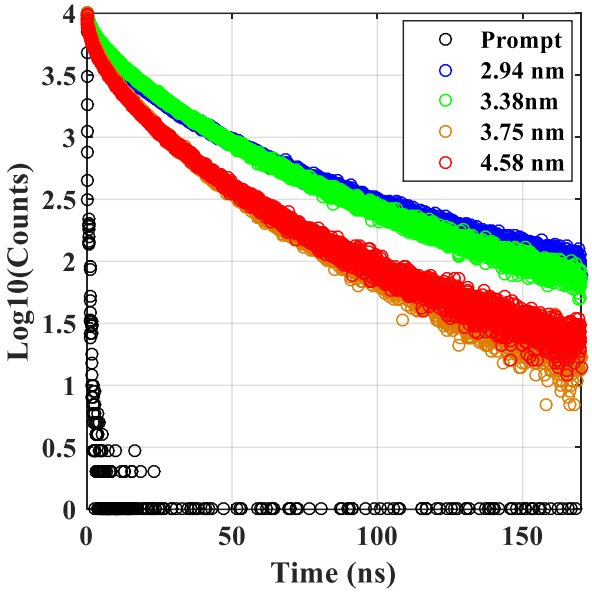

***Figure 2.7**: Fluorescence time decay profile for four different sized CdSe QDs.*

S. No.	QDs size(nm)	T_1(ns)	T_2(ns)	T_3(ns)	A_1	A_2	A_3	T_{avg}(ns)
1	2.94	11.89	0.76	47.08	0.38	0.43	0.20	14.04
2	3.38	12.79	1.13	43.27	0.43	0.35	0.22	15.30
3	3.75	9.78	0.86	32.23	0.39	0.48	0.13	8.51
4	4.58	9.44	0.71	33.73	0.35	0.52	0.13	7.94

***Table 2.2**: Table showing different fitting parameters and time constant values.*

Average lifetime is calculated using following equation for exponential fit:

$$T_{avg} = \frac{A_1T_1^2+A_2T_2^2}{A_1T_1+A_2T_2} \qquad (2.2)$$

2.4.5 Transient Absorption Analysis of CdSe Quantum Dots:

GSB signal is observed at 450 nm and 546 nm corresponding to the steady-state absorption wavelengths. In order study excited state dynamics transient absorption spectroscopy is the most prominent tool since these dynamics cannot be observed using steady state measurements. Signature of steady state dynamics is clearly shown in figure 2.8 at wavelengths 476 nm and 589 nm. For comparison steady-state spectrum is also shown in figure 2.8 (b). The signal at 450 nm and 546 nm is due to the formation of 1P (e)-1P3/2 (h) and 1S (e)-1S3/2 (h) states respectively. Kinetic traces for time decay profile are shown in figure.2.9 and figure2.10 at different wavelengths and kinetic parameters afters bi-exponential fit are shown in table.2.3 and table 2.4.

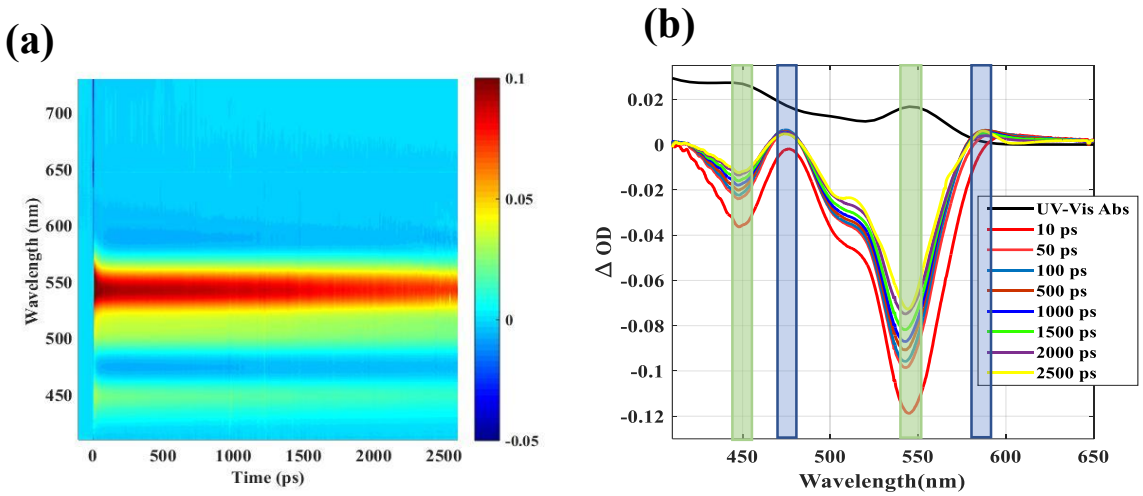

***Figure 2.8**:(a) Spectrally resolved pump-probe data from -100 ps to 2500 ps, (b) steady state absorption and pump-probe data at longer times showing ground state bleach recovery (peach color) and excited state absorption (blue color)*

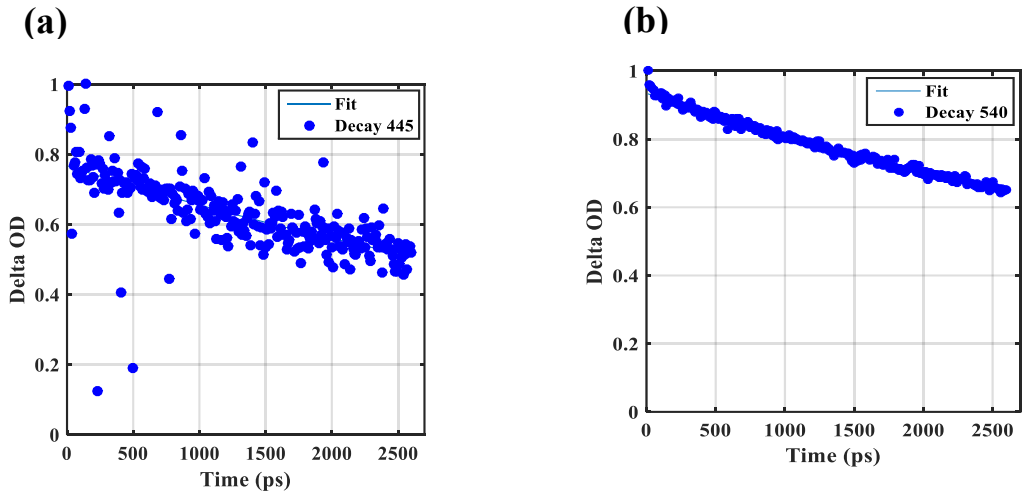

***Figure 2.9**: Kinetic traces for GSB at wavelengths (a) 445nm and (b) 540nm*

Bi-exponential Decay					
	A_1	A_2	T_1	T_1	T_{avg}
445nm	*0.2331*	*0.7669*	*0.1419*	*6368*	*4883.65*
540nm	*0.0658*	*0.9342*	*0.1656*	*7697*	*5675.35*

***Table 2.3**: Table showing different fitting parameters and time constant values*

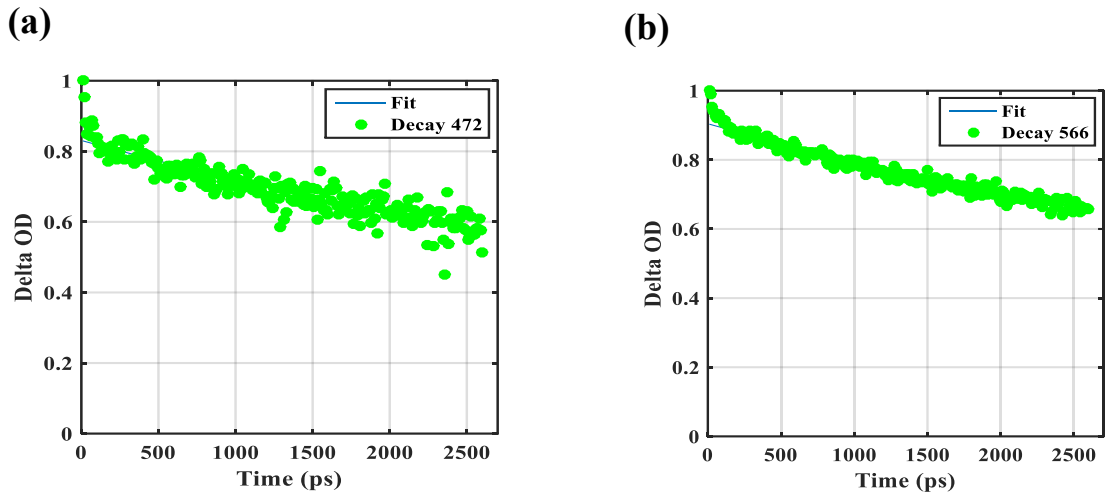

***Figure 2.10**: Kinetic traces for GSB at wavelengths (g) 472nm and (h) 566nm.*

Bi-exponential Decay					
	A_1	**A_2**	**T_1**	**T_1**	**T_{avg}**
472	**0.1692**	**0.8308**	**0.1869**	**6933**	**5759.96**
566	**0.0658**	**0.9342**	**0.1656**	**7697**	**6961.95**

***Table 2.4**: Table showing different fitting parameters and time constant value*

2.5 Characterization of Quantum dots after surface functionalization with cysteine linker

2.5.1 Steady State Absorption

After surface functionalization of CdSe QDs with different concentrations of L-cysteine is shown in figure 2.11. Here we find a slight red shift in absorption maxima as well as fluorescence emission maxima of QDs with increasing concentration of L-Cysteine. This can be possibly because of increase in QDs size after surface passivation which further reduces the QDs bandgap.

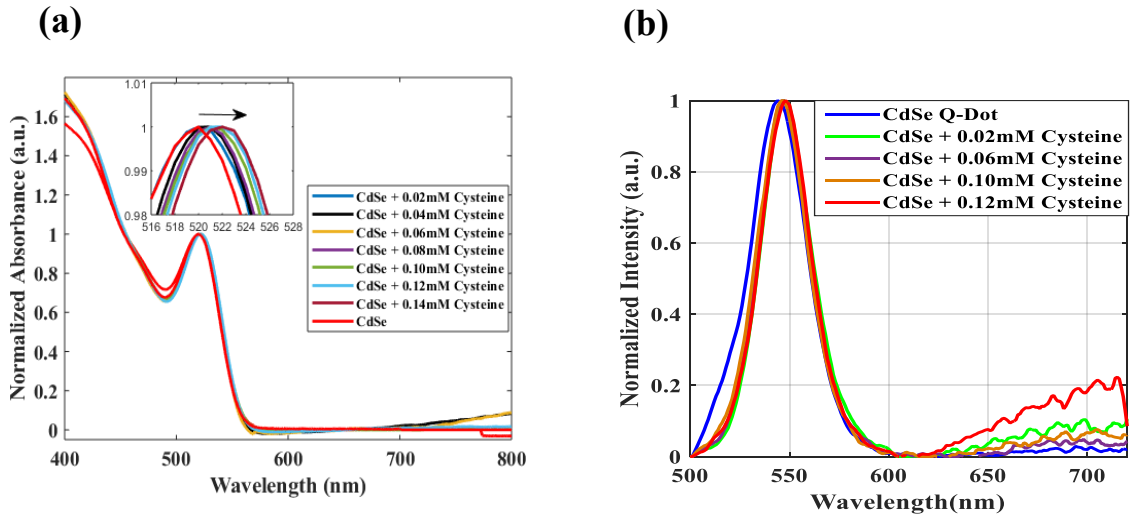

***Figure 2.11**: (a) Steady-state absorption spectra for different sized CdSe QDs after surface functionalization. (b) Steady-state fluorescence emission spectra for different sized QDs after surface functionalization.*

2.5.2 Time resolved fluorescence

Before and after functionalization of QDs fluorescence lifetime parameters after exponential decay fit are shown in table 1.5. Decay profile at different L-cysteine concentration is shown in figure 2.12. The average lifetime remains almost constant after functionalization and this observation is consistent with the observation by Kamat *et. al*[8].

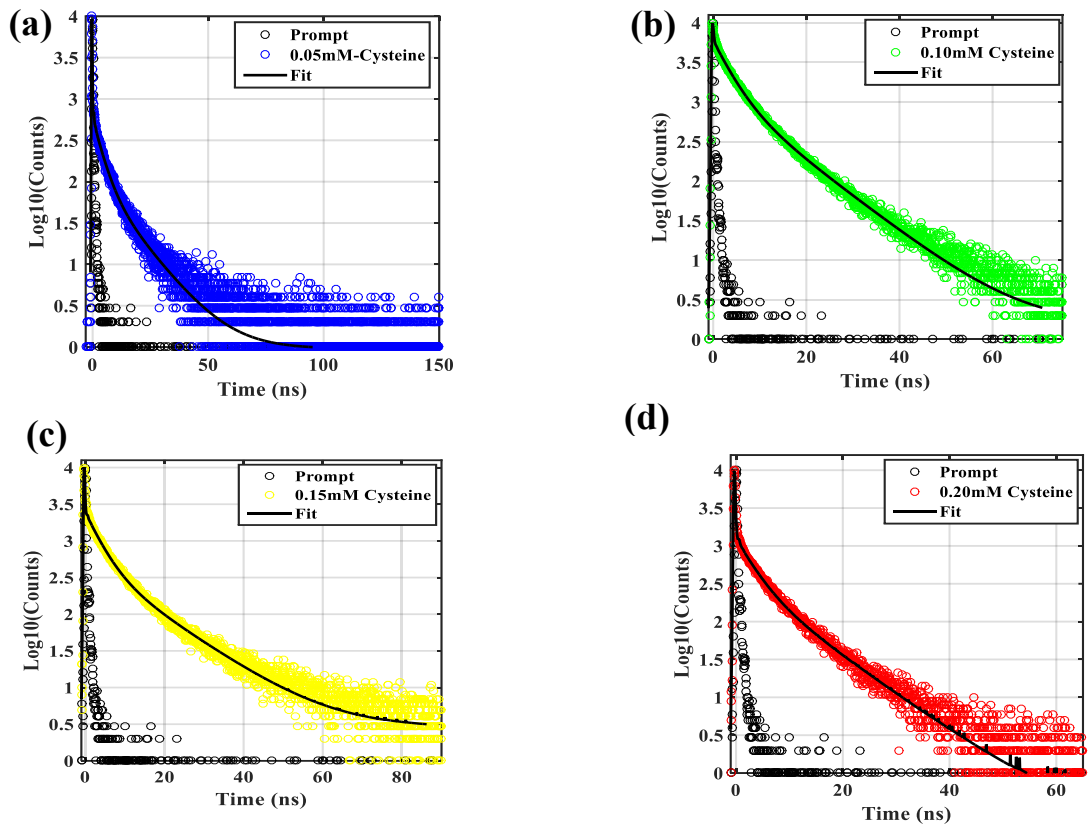

***Figure 2.12**: Fluorescence lifetime decay profiles of CdSe QDs after surface functionalization with different amounts of L-cysteine linker.*

	T_1 (ns)	T_2 (ns)	T_3 (ns)	A_1	A_2	A_3	T_{avg}
QD (2.756)	1.146	36.84	10.6	0.294	0.309	0.432	15.76
0.05mM	0.201	6.04	0.20	0.429	0.052	0.652	0.45
0.10mM	10.93	3.54	0.29	0.108	0.493	0.457	2.89
0.15mM	5.04	0.18	0.18	0.232	0.431	0.414	1.23
0.20mM	0.21	5.02	0.21	0.779	0.114	0.242	0.70

***Table 2.5**: Table showing different fitting parameters and time constant values after exponential decay fit.*

2.6 Conclusion

In summary, highly luminescent CdSe QDs of different size were synthesized using. Without adding any special stabilizing agent, we achieved NIR emitting core only CdSe QDs. Further in order to improve photovoltaic properties of the QDs (by reducing number of surface defects on QDs surface) we did surface functionalization of CdSe QDs with L-cysteine hydrochloride. Surface functionalization allows attachment of cysteine ligands to QD surface, which in turn inhibits recombination of exciton pair generated from CdSe QDs. This process enables more proficient electron transfer from QD to QD via short chain ligand cysteine instead of long chain ligand oleic acid.

Chapter-3

Excited state dynamics of J-aggregates of P3HT polymer nanofibers.

3.1 Introduction

Sunlight is the most abundant source of renewable energy on this planet and several photosynthetic systems have evolved over years to efficiently convert the sunlight into chemical energy. But the harvesting of sunlight for the generation of electrical energy is highly required to meet energy demand. Over the last 50 years, a great development in conversion efficiency of photovoltaic solar cells has been made. Low-cost, low toxicity and large area makes organic photovoltaics a promising candidate where organic semiconducting material (thin layer) is the absorbing material which is sandwiched between two electrodes. Thin film of organic semiconductors shows high absorption coefficient (~ 105 cm^{-1}) and a layer of only 100 nm can absorb up to 90% of incident photons in a double pass using refection from the metal electrode[9-12]. In the past two decades, an extensive research is going on in order to use organic photovoltaic material for solar conversion, and up to 10% of photo conversion efficiency has been achieved for organic solar cells.[13-14]

For the generation of electrical energy, the active layer in a solar cell absorbs the solar light to generate free charge carriers which flow to the electrodes to generate photocurrent. Upon absorption of photon, an electron from the highest occupied molecular orbital (HOMO) of a neutral organic molecule is promoted to the lowest unoccupied molecular orbital (LUMO) and these electron-hole pairs are usually referred to as singlet excitons. Compared to inorganic semiconductors, Frenkel and charge transfer excitons are strongly bound with typical binding energies which have been reported to be between 0.1 and 0.4 eV [15-16].

3.1.1 Conjugated Polymer

Conjugated polymers are often called conducting polymers and in general they have alternate single and double bonds in their chemical structure which offer them special optical and electrical properties. Many classes of conjugated polymers have been synthesized for the optimal performance for their intended application. In 1990s poly para-phenylene vinylene was used for the first time in polymer photovoltaics[17] and polymer light emitting diodes (PLEDs) [18-19] and recently polyfluorenes & polythiophenes have become a good candidate because of their superior performance.

Because of the conjugated π-system, conjugated polymers have impressive optical properties. In these polymers, the π-electrons are not delocalized through the length of polymer backbone, the delocalization is restricted over few monomeric units small segments because of conjugation defects and nature of defect is specific to the different

class of polymers. For example, in polythiophenes these defects occur because of loss of planarity (dihedral angle between two adjacent monomers) over several monomeric units (torsional defects). These defects are randomly distributed throughout the polymer backbone which creates multiple chromophoric units with different energies and these chromophoric units are very sensitive to the functional group of the solvent (e.g. side chains) and environment of the polymer such as solvent in which polymer is dispersed.[20] π -conjugated polymers and their semiconducting as well as non-linear optical properties are widely studied using various spectroscopic tools which helps us to understand how the charged species are formed and charge transfer takes place within these materials when illuminated under light source. Ultrafast spectroscopic studies provide insights into the impacts of electron and hole transfer within these materials for photocurrent generation to construct efficient light harvesting systems. We tried to understand the light harvesting processes like exciton dynamics, within conjugated polymer based functional nanomaterials (P3HT-NF).

3.1.2 Nanowires of P3HT J-aggregates: In recent years the self-assembly of conductive polymer nanowires/nanofibers (NFs) have been studied by many research groups, as they have potential applications in photovoltaics. NFs have a high degree of crystalline order and long-ranged charge transport properties along the NFs axis, which make them promising candidates for organic photovoltaics.

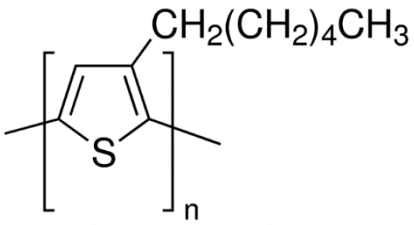

Figure 3.1*: Structure of P3HT polymer*

P3HT polymer is one of the most studied polymers and it has different order of crystallinity in different solvents though preparation methods play a major role. P3HT forms H-aggregates in anisole and J-aggregates in Toluene upon slow cooling which gives fibre like structural morphology. Interchain and Intrachain transport pathways are determined by π–π stacking and the main chain conformation. Molecular weight ($W_{m)}$ also plays an important role in packing/ self-assembly and it has been reported that with increasing molecular weight the backbone conformation is more planar. Charge transport in such polymers occurs either along the backbone which is called intrachain transport or across the π-orbital

coupled with neighbouring polymer chains called interchain transport. The conformation and packing of individual chains comprising the aggregates determines the electronic coupling in π-stacked P3HT aggregates. The charge transport is interrupted by disorders in the assembled /aggregated from. It breaks the delocalization of wavefunction due to weakly or non-overlapping atomic orbitals. In case of P3HT charge transport along the backbone shows higher mobility (almost two times) compared to interchain transport in direction of π–π stacking.

$$\frac{A_{0-0}}{A_{0-1}} = \frac{(1-0.48\mathrm{J}_{k=0}/E_p)\text{^}2}{(1+0.146\mathrm{J}_{k=0}/E_p)\text{^}2} \qquad \text{where exciton bandwidth } W = 2\,|\,J_{k=0}\,| \quad \textbf{(3.1)}$$

For characterization of the complex morphology, the behaviour of such polymers was studied by Spano and co-workers to investigate the polymer aggregates with UV-VIS experiment. Using the model given by them combined with UV-Vis experiment can give information about the orientation of relative transition dipole in polymers which is governed by the alignment of the polymer chain. Spano and co-worker gave the following equation:

By using the above equation, the exciton bandwidth (W) can be determined using the ratio of the vibronic 0-0 transition (A_{0-0}) to the transition 0-1 (A_{0-1}) and both of these transitions are separated by Ep = 0.17eV energy which corresponds to C=C stretching mode (also called phonon energy of coupled phonon mode if Huang-Ray factor is unity). It is known that the exciton bandwidth is determined by the nearest-neighbour interchain coulombic coupling. Since both inter and intra chain coupling is present (competing processes) in aggregated form of P3HT polymers. Both interactions are competitive and one of them can be dominant depending on the crystal size, molecular weight or polymer order. In pure H-aggregates, 0-0 transition is diploe forbidden and shows large exciton bandwidth while this transition is super radiative in J-aggregates.

3.2 Preparation of P3HT-NF

3.2.1 Materials: rr-P3HT was purchased from Sigma Aldrich. Methanol, ethanol, heptane was purchased from Merck, India. Toluene, tetrahydrofuran and methanol were used as solvents. All of the solvents were purchased from Sigma Aldrich, India and used without further purification.

3.2.2 Procedure for P3HT- NF preparation

J-aggregates of P3HT polymer nanofibers were prepared using 1 mg/mL of rr-P3HT in Toluene which is reported in the following research paper[21].This mixture was heated up to 60°C in ultrasonic bath for 30 minutes to fully dissolve rr-P3HT which gives an orange colour to the mixture. Further this mixture was heated up to 80°C and then it was cooled down slowly at a rate of 1°C/4 minutes. For the optical characterization the nanowire suspension was diluted 20 times with mixture of toluene and heptane (1:1) for optical characterization. After centrifugation, the nanofibers were separated from supernatant at 6000 rpm for 15 minutes by adding excess amount of toluene for washing. All the samples were used within two weeks of the preparation of the rrP3HT-NF.

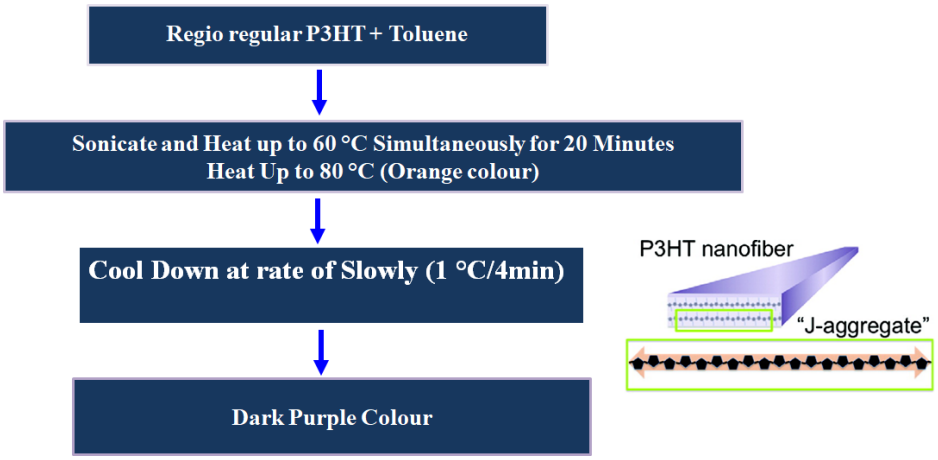

***Figure 3.2**: Schematic for J-aggregates P3HT-NF preparation and packing of Polymer backbone*.

3.2.3 Scanning electron microscope (SEM)

For the characterization of the rrP3HT-NF, the suspension was drop casted on pre cleaned silicon wafers. Before the drop cast, silicon wafers were cleaned with ethanol (twice), Acetone (thrice) and Toluene (twice) respectively. After drop cast these wafers were dried in dark under high vacuum condition.

3.3 Characterization

3.3.1 UV-Vis Spectroscopy

Absorption spectra were recorded in UV-Visible spectrometer (Company Name) in 1 cm quartz cuvette and the Optical Density of the sample was kept between 0.5-1 OD.

3.3.2 Fluorescence Spectroscopy

To record fluorescence spectra, QDs were excited at 520 nm of excitation wavelength in 1 cm quartz cuvette. The sample was diluted enough so that there is no reabsorption.

3.3.3 Scanning Electron Microscope (SEM) image of P3HT-NF

SEM image of P3HT is shown in figure 3.3 and the NF of P3HT polymer coated with gold (Au) on the top of it. These fibres have average diameter of ~16nm.

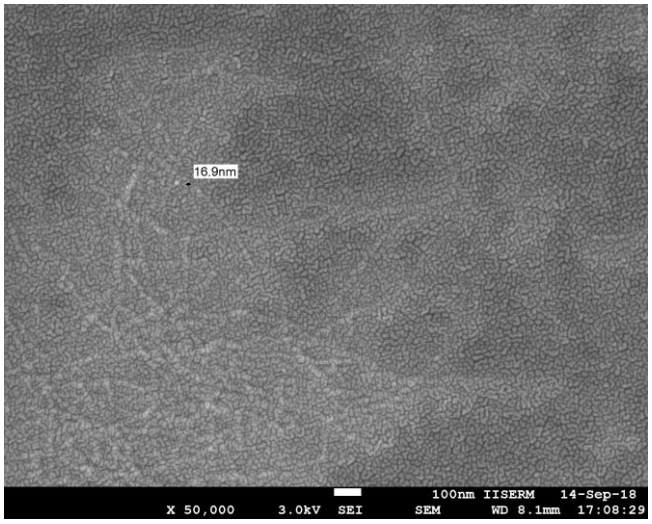

***Figure 3.3**: SEM image of P3HT-NF*

3.4 Results and Discussion

3.4.1 Steady-state absorption

UV-VIS absorption spectra of P3HT in toluene and P3HT-NF dispersed in 1:1 ratio of toluene and heptane is shown in the figure 3.4. Here heptane is used just to preserve the aggregated form of P3HT polymer. There are distinct vibronic progressions in absorption spectra of P3HT-NF and distinct peaks for different vibronic 0-0 (612 nm), 0-1 (565 nm),

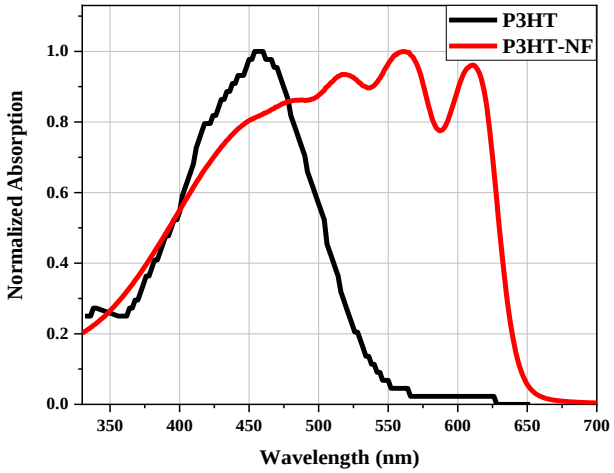

***Figure 3.4**: Normalized UV-VIS Absorption Spectra*

0-2 (525 nm) and the broad peak around 450nm corresponds to the amorphous P3HT which also overlaps with absorption spectra of P3HT (black). Absorption of P3HT-NF before and after purification is shown in the figure 3.5. After purification the broad absorption on blue side of the graph got suppressed significantly**.**

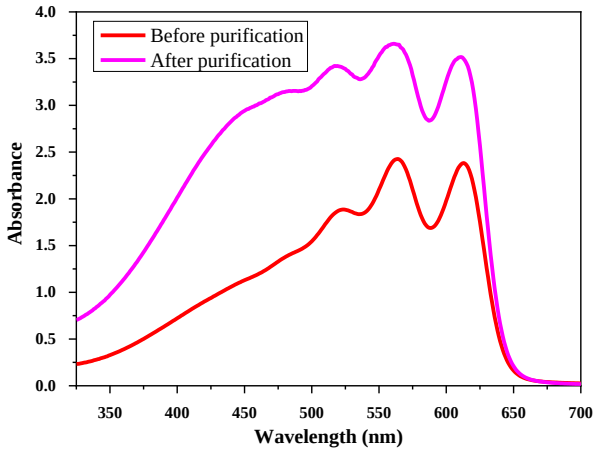

***Figure 3.5**: UV-VIS Absorption of P3HT-NF before and after purification*

Fluorescence spectrum of P3HT-NF which was recorded at an excitation wavelength of 520 nm, is shown if figure 3.6 which is a mirror image of the absorption spectra. Beyond 830 nm the instrument was not sensitive enough and was showing some random noise which has been cropped in the plot.

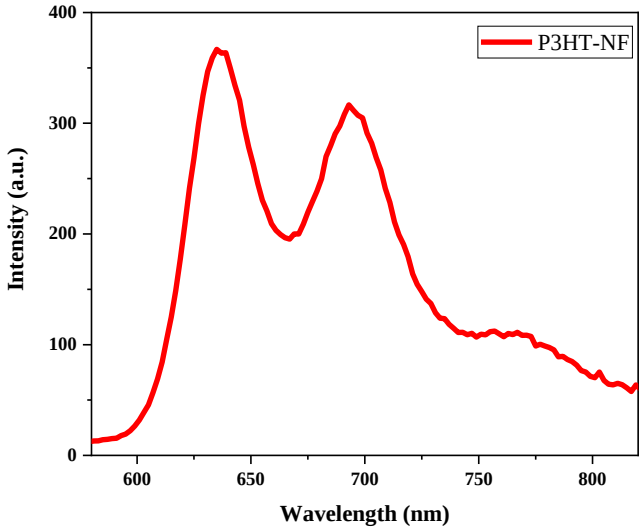

***Figure 3.6**: Steady-state fluorescence emission spectrum of P3HT-NF.*

3.4.2 Deconvolution of absorption spectrum of P3HT-NF: Cumulative fit and the absorption spectra for P3HT-NF is shown in the figure 3.7 and the table for parameters after cumulative fit is table 3.1. The fitting was done using inbuilt multiple peak picking gaussian function in Origin analysis software.

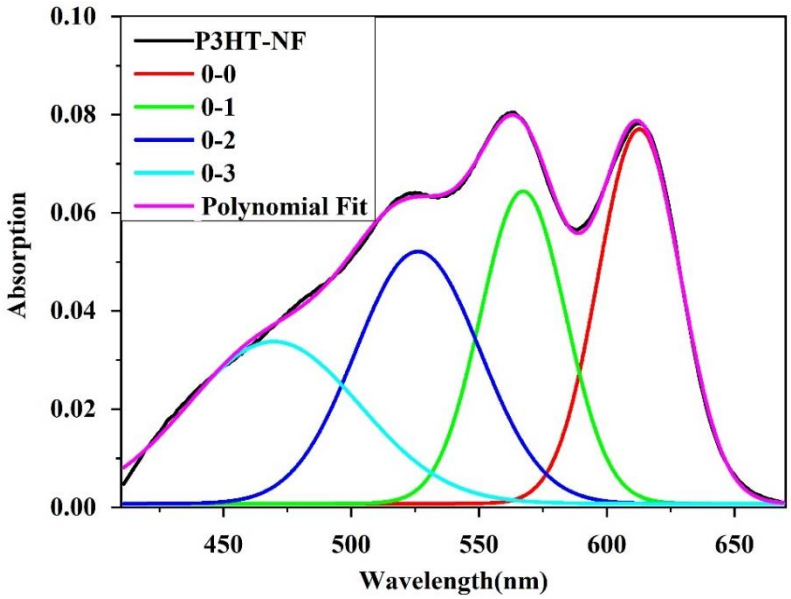

***Figure 3.7**: Cumulative fit and deconvoluted absorption spectra of P3HT NF for different vibrational modes.*

Transition		Value	Standard Error	Transition		Value	Standard Error
Peak-0-0	y0	7.72E-04	2.12E-04	**Peak-0-2**	y0	7.72E-04	2.12E-04
Peak-0-0	xc	**612.74**	0.13	**Peak-0-2**	xc	526.10	0.72
Peak-0-0	A	**3.09**	0.03	**Peak-0-2**	A	3.12	0.32
Peak-0-0	w	38.14	0.28	**Peak-0-2**	w	57.15	2.93
Peak-0-1	y0	7.72E-04	2.12E-04	**Peak-0-3**	y0	7.72E-04	2.12E-04
Peak-0-1	xc	**567.27**	0.35	**Peak-0-3**	xc	469.65	2.52
Peak-0-1	A	**2.65**	0.15	**Peak-0-3**	A	2.79	0.21
Peak-0-1	w	39.22	0.81	**Peak-0-3**	w	79.61	3.17

Table 3.1: *Table for the different parameters after deconvolution fit using gaussian function*

Using the parameter which we got after deconvolution of absorption spectrum of P3HT-NF the ratio of $A_{0\text{-}0}$ /$A_{0\text{-}1}$ came out to be 1.16 and $W = 2 \left| J_{k=0} \right| = 0.038$eV by using $J_{k=0}$ = -0.019eV. The value of $A_{0\text{-}0}$ /$A_{0\text{-}1}$ which is more than unity confirms J-aggregates formation according to the model given by Spano and workers.

3.5 Forster resonance Energy transfer From P3HT-NF to IR-144 Dyes

As an artificial analogue of natural light harvesting system, P3HT play a crucial role in photovoltaic materials. Here we try to study the excitation energy transfer from P3HT-NF to IR-144 dye using long range energy transfer pathway due to spectral overlap.

3.5.1 Forster resonance Energy Transfer:

The Fluorescence Resonance Energy Transfer (FRET) between two molecules is an important a distance dependant radiation less transfer of energy from an excited donor fluorophore to a suitable acceptor fluorophore. Due to its sensitivity to distance, FRET has been used to nearby acceptor fluorophore through long range dipole-dipole interaction in non-radiative fashion.

3.5.2 Spectrum Overlap between Emission of Donor (P3HT-NF) and Absorption of Acceptor (IR-144):

After purification of P3HT-NF they were dispersed in 1:1 ratio of Tetrahydrofuran (THF) and heptane. Again, here heptane is used just to preserve the aggregated form of P3HT polymer. IR-144 (50nM) was also dissolved in in the same ration of THF and Heptane. In order to confirm the required condition for FRET we checked for the spectral overlap between emission spectrum of P3HT-NF and absorption spectrum of IR-144. As we can see from the figure:3.8. that there is reasonably good overlap the spectrum in order of form FRET in the system.

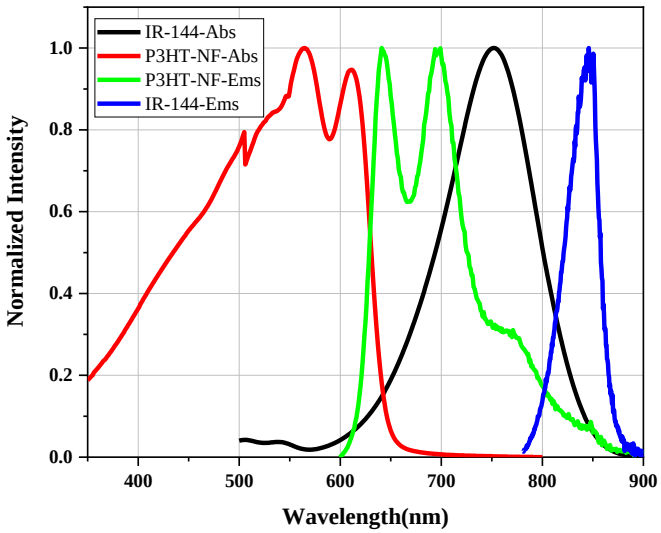

***Figure 3.8**: Absorption & Fluorescence spectrum of P3HT-NF & IR-144*

3.5.3 Fluorescence Quenching of P3HT-NF in presence IR-144:

In order to study the fluorescence quenching of P3HT-NF which ideally should occur in our system because of excited sate energy transfer from P3HT-NF to IR-144, the concentration of IR-144 was increased and the amount of P3HT-NF was kept constant in a fixed total volume.

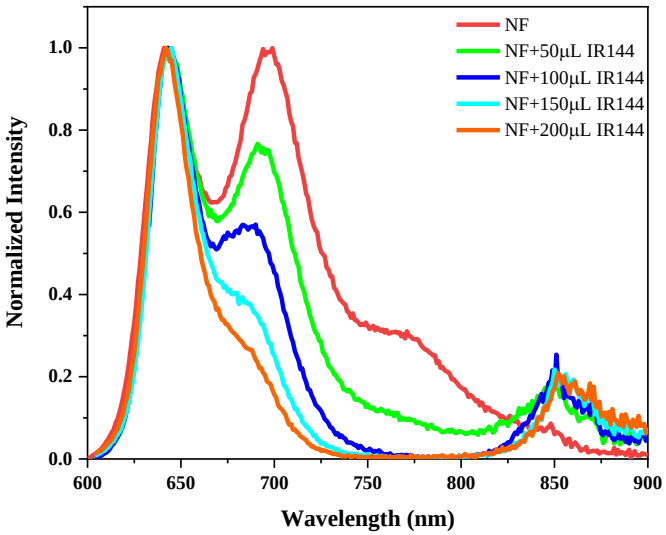

***Figure 3.9**: Fluorescence spectra of P3HT-NF in presence different concentration of IR-144.*

520nm wavelength was used in order excite P3HT-NF and the emission was recorded in range of 600-900nm. Here we see that the fluorescence quenching is taking place around 700nm wavelength region. But corresponding to that there must be a significant increase in the emission of IR-144 (at 850 nm wavelength) which we couldn't see here. So, from here we conclude that the fluorescence quenching of P3HT-NF is not taking place because of FRET. The possible reason can be the aggregate formation of P3HT-NF with IR-144 or some other process may be present these which is may cause quenching. After the failure of this experiment we moved to the excited sate characterization of P3HT-NF using pump-probe spectroscopy.

3.6 Transient absorption study of P3HT-NF

Transient absorption spectroscopy (TAS) of P3HT-NF in solution phase was done by exciting the sample at 520 nm output pump pulse generated by NOPA (Nonlinear optical parametric amplification) and white light as probe. TAS technique allows the direct study of NF chain packing characteristic of these dynamics and provides reliable information about excitonic coupling. In the study of polymer aggregates the key advantage of using TAS is that these measurements are not affected by self-absorption and line shape distortion are specially in case of J-aggregates.

Pump-probe signal as function of pump-probe delay and probe wavelength is shown in figure 3.10.

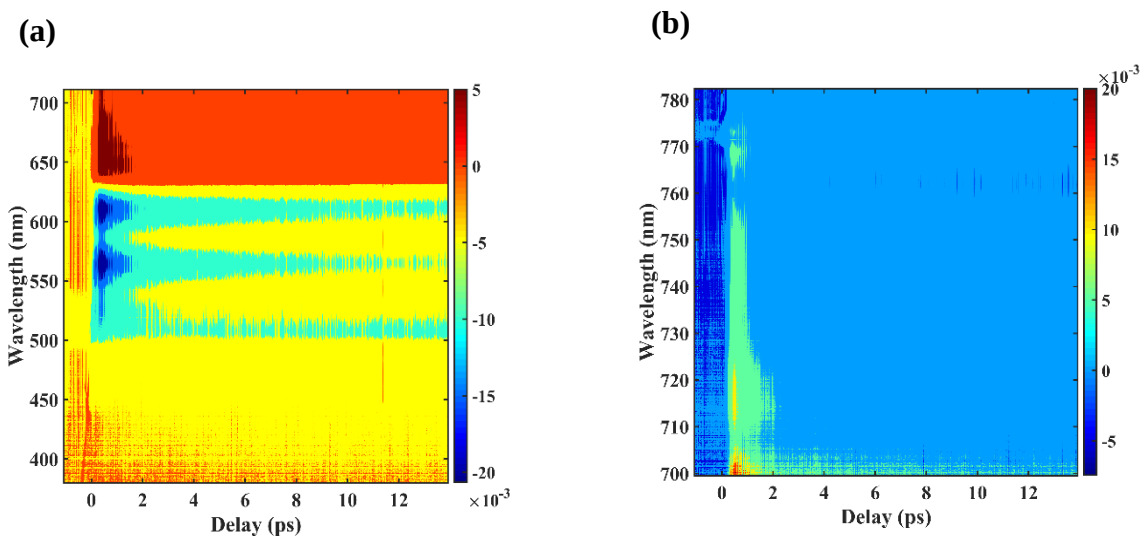

***Figure 3.10**: Pump-probe signal as function of pump-probe delay and probe wavelength in the range of (a) 480-710 nm (b) 700-785 nm*

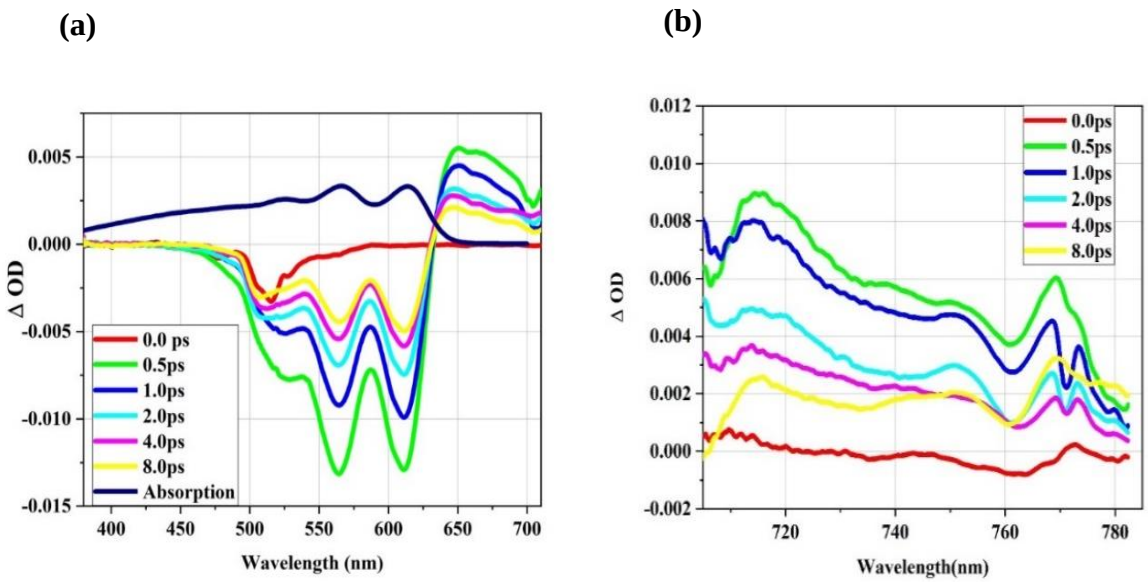

Figure 3.11: Spectral traces for pump probe signal with varying time delay at 520 nm pump excitation. (a) GSB-612 nm & ESA-660 nm (c) ESA centered around 750 nm.

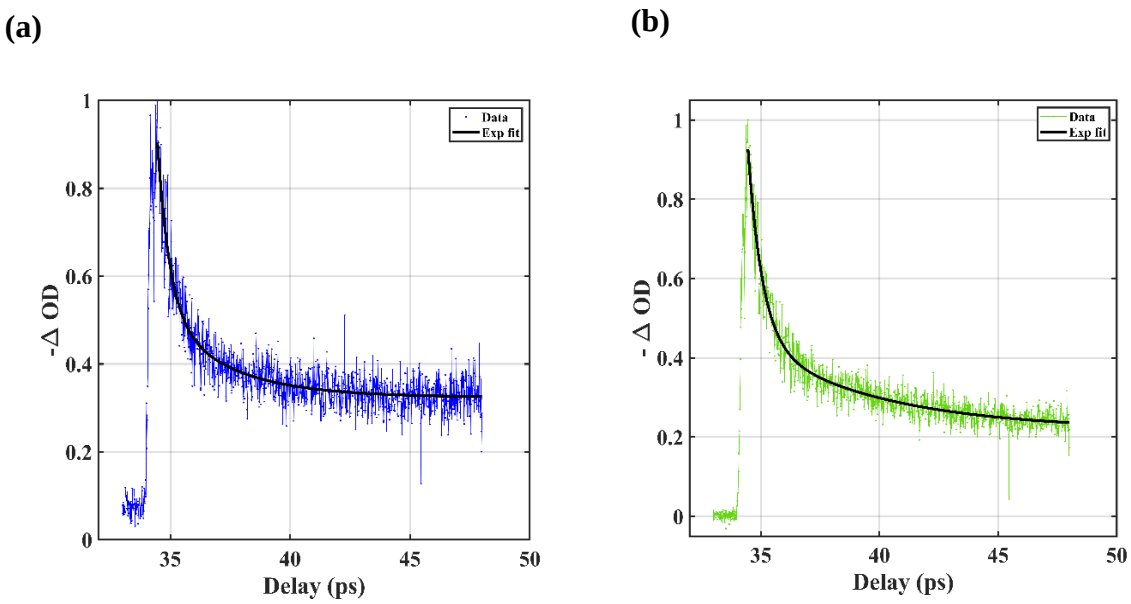

***Figure 3.12**: Normalized TA kinetic traces with exponential decay fit for ground state bleach GSB (a) 525nm (b) 565nm*

	Bi-exponential fit	
P3HT-NF	**525 nm**	**565 nm**
A1	**0.50**	**0.55**
t1 (ps)	**0.51**	**0.61**
A2	**0.21**	**0.23**
t2 (ps)	**2.80**	**5.39**

***Table3.2**: Table for decay parameters for GSB at 525nm and 565nm*

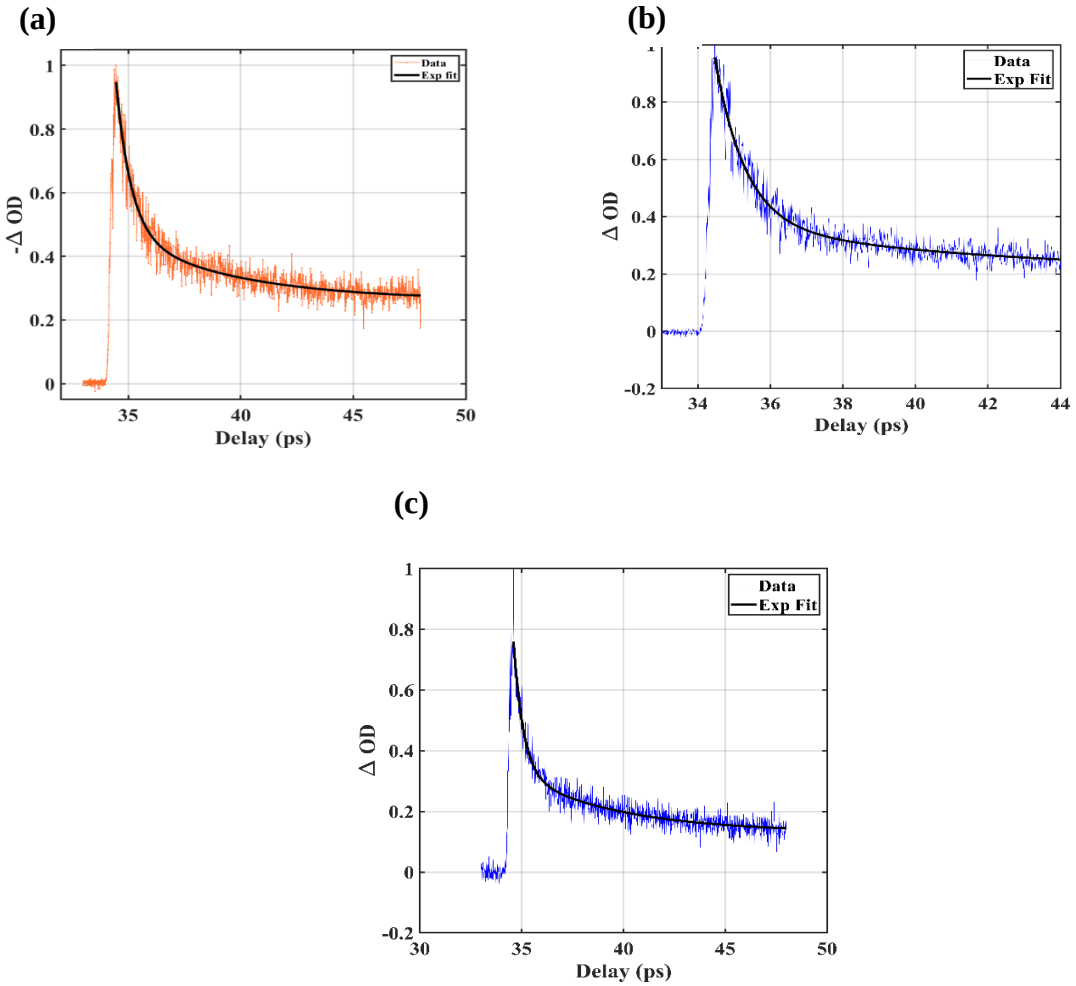

***Figure 3.13**: Normalized TA kinetics trace with exponential decay fit for ground state bleach GSB signal at (a) 612 nm corresponding to Polaron Pair (PP) (b) 660 nm corresponding to Delocalized polarons (c)760nm*

P3HT-NF	612 nm	660 nm	760 nm
A1	0.53	0.314	0.836
t1 (ps)	0.68	0.811	0.298
A2	0.22	0.489	0.250
t2 (ps)	5.01	17.07	3.409

***Table 3.3**: Table for decay trace parameters for GSB at 612nm, PP at 660nm and DP at 750nm wavelength.*

In solution phase of P3HT-NF the signals correspond to structural relaxation and autoionization. In visible spectral probe range, there are mainly three types of signals, GSB (525 nm, 565 nm and 612 nm), PP (660nm) and DP signals which appears at $\lambda > 725$nm. The GSB signal completely matches with the steady-state absorption signal of the excited population. Here we observe that all the signals for J-aggregates decay at very fast time scales(1-20ps) which is very less if we compare with the normal decay lifetime of amorphous P3HT. For amorphous P3HT typical decay time which have been reported in literature goes up to 2-3 ns. Not only in J-aggregates of P3HT, H-aggregates of P3HT also shown very fast time decay which is even faster than J-aggregates of P3HT. Grey and co-workers[21] said that the possible reason for the fast decay in packed systems (J- and H-aggregates) is because of very fast torsional relaxation.

3.7 Conclusion

In summary, J-aggregates of P3HT polymers were prepared and their steady state optical characterization was done. J-aggregate formation of the polymer was confirmed by using the empirical formula derived from theoretical model given by Spano and co-workers. FRET study was also performed from P3HT-NF(Donor) and IR-144 (Acceptor) but we found that fluorescence quenching in P3HT-NF was not occurring because of energy transfer from P3HT-NF to IR-144. Further to investigate excited state dynamics of P3HT-NF, Transient Absorption Spectroscopy was performed where excited state species polaron pair and delocalized polaron were observed at 650nm and $\lambda > 725$ nm respectively which can't not be observed in steady state measurements. These species further confirm charge mobility in two direction (within the chain and between the chains) in packed structure of P3HT-NF.

BIBLIOGRAPHY

1 J. Dana, P. Anand, S. Maiti, F. Azlan, Y. Jadhav, S. K. Haram, H. N. Ghosh, J. Phys. Chem. C 2017, Articles ASAP (As Soon As Publishable), DOI: 10.1021/acs.jpcc.7b08448

2 Halder, G.; Ghosh, D.; Ali, M. Y.; Sahasrabudhe, A.; Bhattacharyya, S. Interface Engineering in Quantum Dot Sensitized Solar Cells. Langmuir 2018, DOI: 10.1021/acs.langmuir.8b00293.

3 K. Zhao, Z. Pan and X. Zhong, J. Phys. Chem. Lett. 2016, 7, 406–417.Xi. Zhang, P. K. Santra, L. Tian, M. B. Johansson, H. Rensmo, and E. M. Johansson, ACS Nano, 2017,11, 8478–8487

4 C. H. Chuang, P. R. Brown, V. Bulović, M. G. Bawendi, Nat Mater. 2014, 13, 796-801.

5 L. Qu and X. Peng, J. Am. Chem. Soc., 2002, 124, (9), 2049-2055.

6 L. Qu, Z. A. Peng, and X. Peng, Nano Lett., 2001, 1 (6), 333-337.

7 . W. W. Yu, L. Qu, W. Guo and X. Peng, Chem. Mater., 2003, 15, 2854-2860.

8 D. A. Hines and P. V. Kamat, J. Phys. Chem. C, 2013, 117, 14418-14426

9 Kippelen, B.; Bredas, J.-L. Organic Photovoltaics. Energy Environ.Sci. 2009, 2 (3), 251−261.

10 1Lu, L.; Zheng, T.; Wu, Q.; Schneider, A. M.; Zhao, D.; Yu, L. Recent Advances in Bulk Heterojunction Polymer Solar Cells. Chem. Rev. 2015, 115 (23), 12666−12731.

11 Brabec, C. J.; Gowrisanker, S.; Halls, J. J. M.; Laird, D.; Jia, S.; Williams, S. P. Polymer−Fullerene Bulk-Heterojunction Solar Cells. Adv. Mater. 2010, 22 (34), 3839−3856.

12 Deibel, C.; Dyakonov, V. Polymer−fullerene Bulk Heterojunction Solar Cells. Rep. Prog. Phys. 2010, 73 (9), 096401.)

13 Brabec, C. J.; Gowrisanker, S.; Halls, J. J. M.; Laird, D.; Jia, S.; Williams, S. P. Polymer−Fullerene Bulk-Heterojunction Solar Cells. Adv. Mater. 2010, 22 (34), 3839−3856.

14 Deibel, C.; Dyakonov, V. Polymer−fullerene Bulk Heterojunction Solar Cells. Rep. Prog. Phys. 2010, 73 (9), 096401.

15 (7) Alvarado, S. F.; Seidler, P. F.; Lidzey, D. G.; Bradley, D. D. C.

16 Direct Determination of the Exciton Binding Energy of Conjugated Polymers using a Scanning Tunneling Microscope. Phys. Rev. Lett. 1998, 81 (5), 1082−1085.

17 Tsutsumi, J. y.; Matsuzaki, H.; Kanai, N.; Yamada, T.; Hasegawa, T. Charge Separation and Recombination of Charge-Transfer Excitons in Donor-Acceptor Polymer Solar Cells. J. Phys. Chem. C 2013, 117 (33), 16769−16773

18 Sariciftci, N.S., Smilowitz, L., Heeger, A.J. and Wudl, F., *Science*, **1992**, 258, 1474-1476.

19 Burroughes, J.H., Bradley, D.D.C., Brown, A.R., Marks, R.N., Mackay, K., Friend, R.H., Burns, P.L. and Holmes, A.B., *Nature*, **1990**, 347, 539-541.

20 Grage, M.M.L., Pullerits, T., Ruseckas, A., Theander, M., Inganäs, O. and Sundström, V., *Chemical Physics Letters*, **2001**, 339, 96-102.

21 Edwards T. Niles, John D. Roehling, Hajime Yamagata, Adam J. Wise, Frank C. Spano, Adam J. Moulé, and John K. Grey., J. Phys. Chem. Lett., 2012, 3 (2), pp 259–263.